INTUITIVE ITN MSCA - Deliverable D4.5
Soft MEMS based stress and slip sensors
ESR 10 Inci Rüya Temel

Prepared within the Foundation Bruno Kessler, Italy, under the supervision of Leandro Lorenzelli and the co-supervision of Andrea Adami

Submitted the 10 November 2023 with some delay due to missing results. This first version will be updated at the end of the project as my contract has been extended until the end of the project.

Chapter 1. Introduction

Humans are capable of highly skilful movements, such as playing musical instruments, crafting tools, or producing art. Therefore, humans can create, remodel the world around them, and interact socially. All behavioural patterns arise from the tight coordination of the nervous system with the body and environment [1]. Many motor control studies have highlighted the importance of sensory feedback in achieving the dexterous manipulation of objects [2]–[4]. An accurate manipulation task requires information not only on the body's current state, but also on the object's physical properties such as shape, weight, position, and temperature. The human brain is a powerful machine that can predict these parameters and is capable of perceiving the impedance of objects, such as their stiffness, damping, and inertia, through the integration of motion and force signals [5]–[8]; however, it is subject to many errors. The fundamental step before planning, learning, and adapting future movements to the environment's current state is to sense them through vision, but most essentially through touch.

Extensive work has been conducted by Professor Johansson and his team from the University of Umea, Sweden. They have been involved in early research on mechanoreceptors, identifying their receptive field characteristics [8], measuring their densities [9], and their spatiotemporal properties [10]–[12] in the 1970s and the 1980s. Their work led them to identify the mechanisms of precision gripping when lifting objects [13].

FIGURE 1 shows the different steps in sensing contact and adapting the grip according to the physical properties of the object. Tactile afferent signals were recorded during the lifting tasks. These recordings show that all four types of mechanoreceptors participate in the task, allowing the brain to monitor the progression of the task to correct any errors that can occur before the end of the lifting task. Primarily, when the fingers enter in contact with the object, FA-I (fast adapting type I) afferents fire, giving the information of the contact, along with FA-II (fast adapting type II) afferents responding to transient mechanical events when the object is lifted

and then replaced. Secondly, during all the time a static force is applied in order to hold the object, slow-adapting fire continuously.

This work shows the importance of developing an electronic skin that is capable of detecting dynamic signals as well as static signals, but more importantly, to integrate shear force sensors along the existing pressure sensors that are not sufficient to adapt the applied force in case of unsuccessful handling.

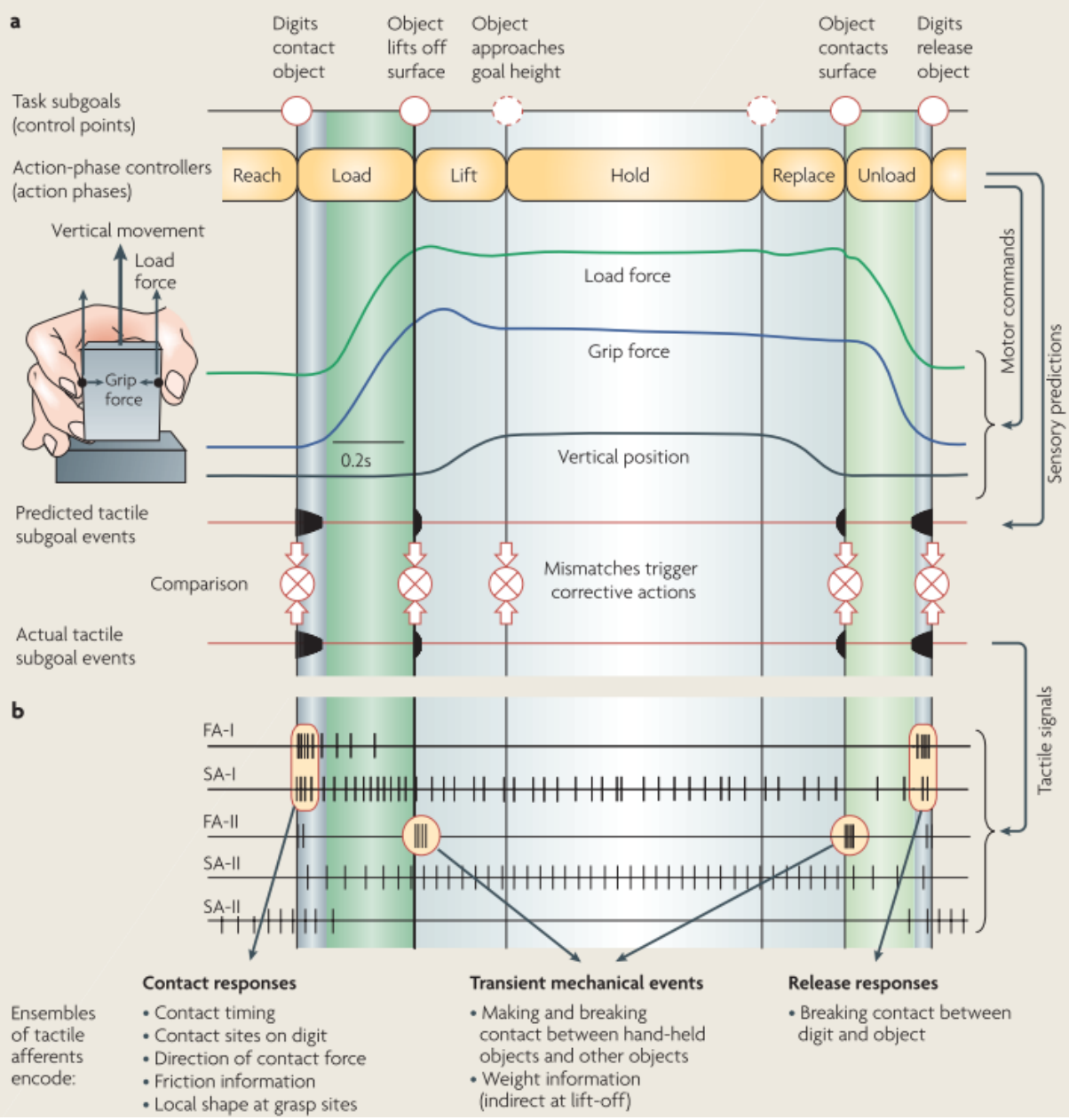

FIGURE 1 SENSORY EVENTS DURING A LIFTING TASK. (a) Identification of goals and measurement of forces applied to reach the goal; (b) measurement of signals recorded from the four mechanoreceptors. [4]

Chapter 2. Context and background

2.1 Inspirations from the human skin

The tactile sensing emerges from the contact of two physical bodies. In neurosciences, it refers to the conscious contact of the human body with the environment. The skin, which is the interface between the word and the body, is composed of seven types of sensory receptors: thermoreceptors, receptors that detect humidity, nociceptors, and four types of mechanoreceptors [14].

Mechanoreceptors in the hand can be classified based on their receptive field and response time to a stimulus. Type I receptors have small and well-defined receptive fields and are located in the superficial layers of the skin. Type II receptors have large, ill-defined and roughly uniform receptive fields and are terminated deeper in the dermis and the epidermis [8]. Each type includes both fast adapting and slowly adapting receptors. Fast adapting (FA) receptors are sensitive to dynamic skin indentation, as long as the stimulus is in motion, and stop firing when the stimulus becomes stationary. Slowly adapting (SA) receptors are also sensitive to moving stimuli but respond to a maintained skin indentation during static pressure with a sustained discharge [15]–[18]. FIGURE 2 represents the different mechanoreceptors located in the skin and their temporal response to stimulus.

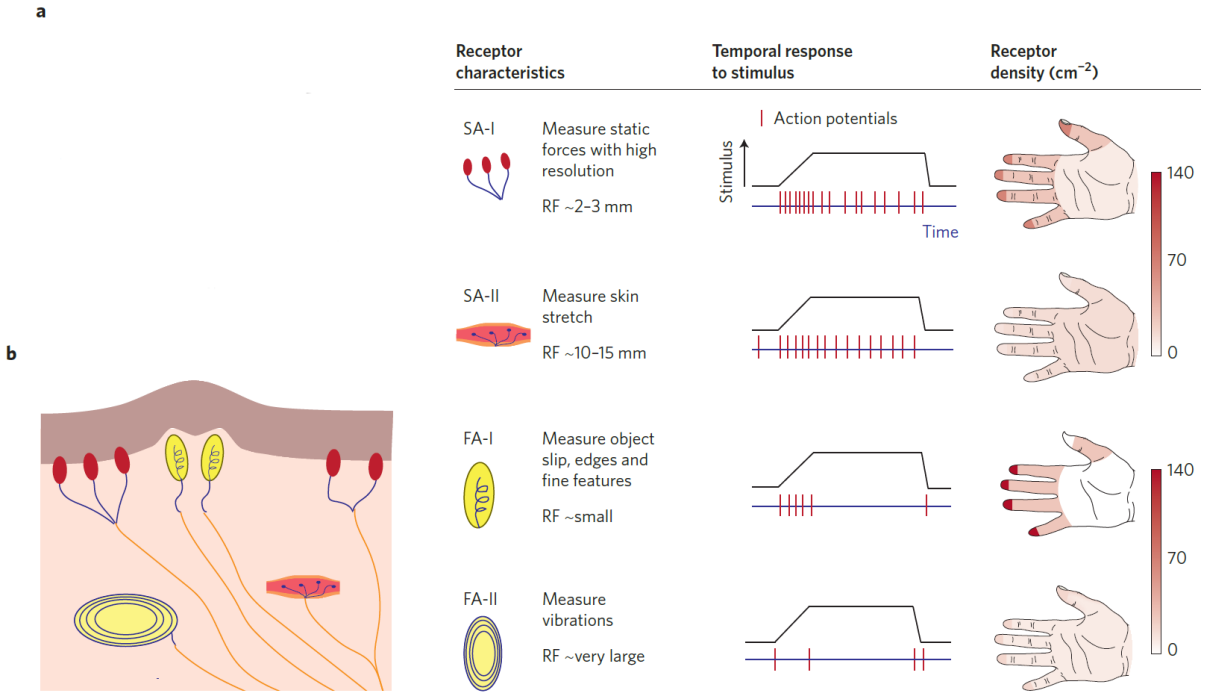

FIGURE 2 SKIN RECEPTORS AND TRANSDUCTION PROCESS. A, Types of mechanoreceptors, their function, temporal response and density in the hand. b. Schematic of the location of mechanoreceptors in the skin. [19]

Mimicking the humans' ability to dexterously manipulate objects requires sensors arrays to measure normal and shear force distributions and orientations. In tasks such gripping, all four mechanoreceptors are involved. While slow adapting receptors transduce static force, fast

adapting receptors are engaged in order to transduce dynamic force. Thereby, both static and dynamic force transduction are required to detect shear stress and strain. In addition, number and diversity of different sensors are important parameters to include in order to build an electronic skin capable of detecting slip and allowing efficient grip. Furthermore, fingertips have a high spatial resolution and can perceive pressure changes as low as 2 kPa. The TABLE 1 gives the main features of the four mechanoreceptors in the skin.

Classification basis		**Pacinian corpuscle**	**Ruffini corpuscle**	**Merkel Cells**	**Meissner's corpuscle**
Type		FA II	SA II	SA I	FA I
Adaptation rate		Fast	Slow	Slow	Fast
Spatial acuity (mm)		10+	7+	0.5	3-4
Vibration/ rapid indent. threshold	*Best (μm)*	0.01	40	8	2
	Mean (μm)	0.08	300	30	6
Stimuli Frequency (Hz)		40-500	100-500	0.4-3	3-40
Conduction Velocity (m/s)		35-75	34-70	40-65	34-70

TABLE 1 CLASSIFICATION AND PROPERTIES OF THE FOUR MECHANORECPTORS IN THE SKIN [15], [20]

Designing an active robotic prosthesis can be a great challenge, having in mind how difficult it can be to provide sensory feedback. Skin is the largest organ of the body, and is stretchable up to 75% its strain. Considering to cover prosthetics with electronic skins is to consider a design that allows free movements as much as a design easy to fabricate and replicate, minimizing its per-area cost [19].

Besides, users' acceptance their artificial limb depends on how good the artificial limb can mimic the impaired limb, but also how easy it is to use it, including its weight, cost, durability and appearance [21]–[24]. First, a skin-like coverage that looks and feels like the real skin may improve comfort and social acceptance. Second, providing sensory feedback from the artificial limb may improve the perception of ownership of the new limb. Additionally, completing the lacking limb with artificial sensory pathways can alleviate phantom limb pain. Third, sensory feedback is essential for optimal and successful manipulation. However, it may ease the utilisation of the prosthetic limb by restoring information about proprioception and grip forces.

To meet these requirements, future electronic skin aims to improve the following key performance parameters: sensitivity, dynamic range, response time, relaxation time, and detection limit. TABLE 2 lists the requirements for the bioinspired electronic skin.

Parameter	Requirements for electronic skin
Force direction	Both normal and tangential
Force range	4 – 200 kPa
Temporal variation	Both dynamic and static
Time response	10 ms
Spatial resolution	1mm at fingertips, 5mm on palm, even less on limbs and belly
Sensor output	Stable, repeatable, monotonic and low hysteresis
Sensing surface	Compliant and durable
Mechanical properties	Flexible, conformable, stretchable and robust (depending on the application and environment)
Shielding	Electronic and magnetic shielding
Data organization	Pre-processing to reduce data to central unit
Fabrication	Simple mechanical integration, minimal wiring, low cost
Electronics	Low power consumption

TABLE 2 REQUIREMENTS FOR ELECTRONIC SKIN FOR PROSTHETIC APPLICATION

2.2 Recreating sensation of slip in artificial limb

2.2.1 Static force and strain transduction.

In the field of force and strain transductions, various mechanisms are employed, with capacitive and resistive approaches being particularly common. Capacitive sensors rely on changes in capacitance, which occur when two electrodes separated by a dielectric layer experience movements. On the other hand, resistive sensors generate an output signal through either measuring the intrinsic material piezoresistivity or detecting changes in contact resistance between a conductor and an electrode [25]. To delve deeper into the working mechanisms of resistive and capacitive sensing, the following section will provide a more detailed explanation on the rationale behind the choice to work with a capacitive sensor.

Numerous studies in the literature have reported numerous sensors that demonstrate sensitivities equal to or better than that of human skin. Notably, both capacitive and resistive sensors offer improved detection thresholds compared to the skin. While the skin's detection threshold stands at 1 mN, those of capacitive and resistive sensors are respectively smaller than 0.05 mN and 0.08 mN. Furthermore, both capacitive and resistive sensors can achieve significantly enhanced response times. It can reach less than 10 ms and less than 20 ms for devices based on capacitance and resistance, respectively. In comparison, the skin's response time is approximately 15 ms.

The resistive sensor consists of a conductive material placed on a substrate. Their simple structure has also a simple working principle which is based on a variation of the resistivity of the conductive material in response to different magnitude of applied pressure. In general, the resistance goes by decreasing as a given pressure is applied increasingly. Piezoresistive sensors able to detect normal force, shear force, lateral stretch and bending have been successfully shown in the literature. Park et al. [25] developed in 2014 their simple bioinspired interlocked microstructures using only PDMS and carbon nanotubes as represented in the FIGURE 3.

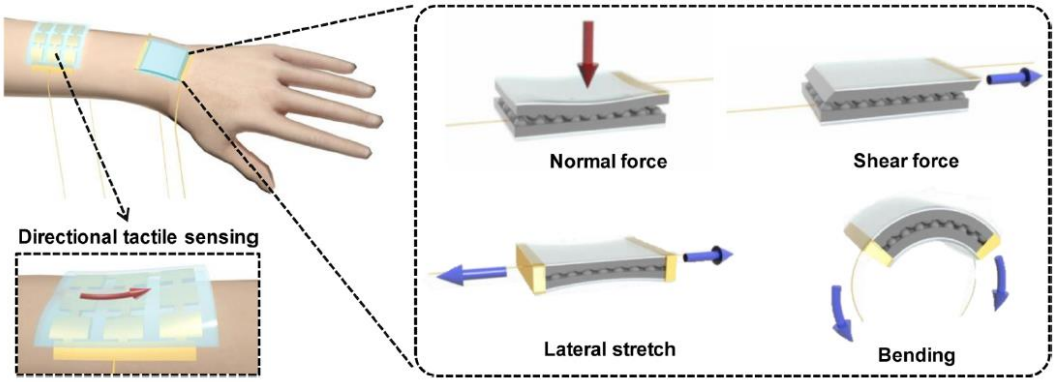

FIGURE 3 ELECTRONIC SKIN BASED ON CARBON NANOTUBE POLY(DIMETHYLSILOXANE) (CNT PDMS) COMPOSITE FILMS WITH INTERLOCKED. Schematic of a stress-direction-sensitive electronic skin for the detection and differentiation of various mechanical stimuli including normal, shear, stretching, bending, and twisting forces. [25]

The capacitive sensor consists of two parallel plate electrodes which are separated by a dielectric layer. Its working principle remains on the change of capacitance due to applied force [26]. A change of capacitance will be observed either when the distance between the electrodes change, or when the overlapping area between the two electrodes is modified, or else when the relative permittivity of the dielectric will change. [27] Capacitive sensors able to detect normal force and shear force have been successfully shown in the literature.

In theory, for the same given amount of deformation due to applied pressure, the output signal demonstrates a greater change in resistive-type sensors than in capacitive sensors, leading to a wider dynamic range in the former. Furthermore, resistive sensors possess a simpler readout mechanism, which adds to their appeal. However, their cost-efficiency is low due to their constant and high power consumption and are more difficult to fabrication since novel materials have to considered in order to be able to observe wide range of conductivity change. Because capacitive sensors are comparatively easier to fabricate, exhibit fast response times and require lower power consumption [28], they are better suited for skin-like sensing capabilities. Additionally, they can be readily integrated with energy conversion and storage devices such as supercapacitors or solar cells [29].

Resistive-type sensors have the disadvantage to use non-stretchable materials to be able to obtain high resolution. Intrinsically stretchable materials can be used by mixing them with percolating CNT network [30] or designing them such as microfluidic liquid metal channels [24]. However, a trade-off has to be made between conductivity and stretchability as reducing percolation pathways reduces conductivity, but increasing percolation pathways reduces stretchability. Although they have low operating voltage and high sensitivity, piezoresistive polymer composites exhibit large hysteresis, large confounding temperature sensitivity, and poor pressure sensitivity.

The capacitive sensors present the advantage of being able to detect both static pressure and strain, making them very suitable for an electronic-skin [31]–[34]. For example, Bao et al. [35] have successfully designed a capacitive sensor with high resolution and sensitivity using microstructures, as shown in the **FIGURE 4**. Besides, they demonstrate excellent sensitivity and linearity, making their response fast while requiring low power consumption and being temperature-independent. However, they need to be shielded to reduce their susceptibility to external noise sources from electromagnetic waves. Moreover, the viscoelastic nature of rubber dielectrics increases hysteresis. But this latest disadvantage can be overcame by micro-engineering the dielectric layer as we are going to see later.

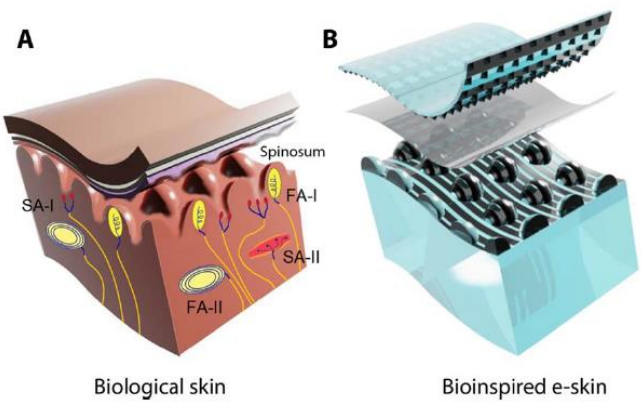

FIGURE 4 HUMAN SKIN INSPIRED E-SKIN USING CAPACITIVE SENSING MECHANISM. (A) Cross-section of the skin from fingertip depicting key sensory structures. (B) Soft biomimetic e-skin. Black, CNT electrodes; blue, PU elastomer; grey, intermediate thin-film dielectric layer, which ensured electrical insulation of the capacitors. Each hill corresponds to 25 capacitors. [35]

2.2.2 Dynamic force transduction.

Dynamic sensing can be mimicked thanks to piezoelectric and triboelectric sensors which produce a voltage when they are mechanical deformed, causing change in the magnitude of dipoles in the active layer and inducing the electrodes to charge [19]. The difference between piezoelectric and triboelectric materials reside in the mechanism leading the dipole to charge. In piezoelectric materials, the application of strain can change either the magnitude of the dipole in the unit cell or the number of dipoles per volume of material. In triboelectric devices, dipoles are induced by contact electrification, in which charges are separated because of a difference in work function between two materials. These sensors are selectively sensitive to dynamic pressures, making them suitable for mimicking the properties of FA-I and FA-II receptors [15]. Finally, the working principle of piezoelectric and triboelectric sensors allows them self-powering due to the energy produced by mechanical stimulation [36].

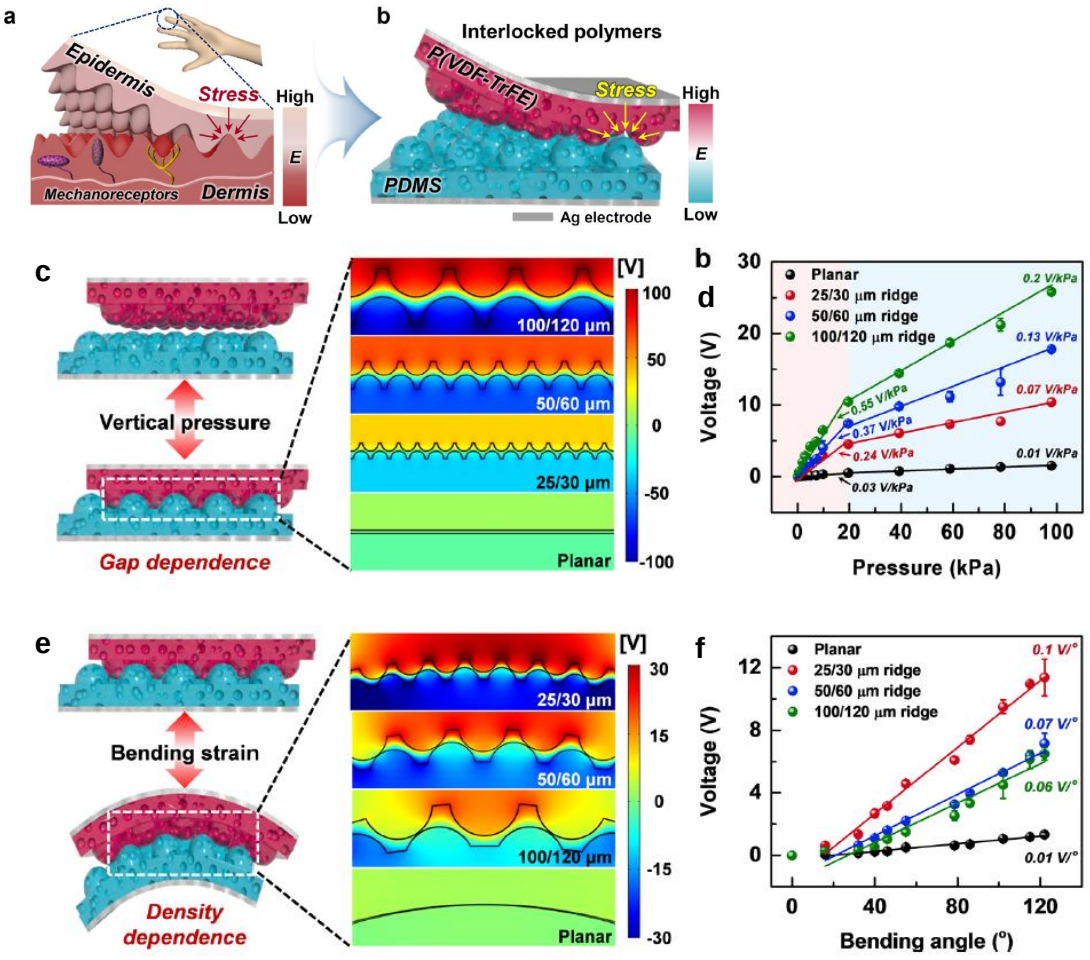

FIGURE 5 SKIN-INSPIRED AND HIERARCHICAL POLYMER ARCHITECTURES FOR SPACER-FREE, ULTRATHIN, AND HIGHLY SENSITIVE TRIBOELECTRIC SENSORS (TESS). (a) Structural and functional characteristics of human skin. The different elastic modulus (E) of epidermis–dermis layers with interlocked microridges effectively transfer the external stress to underlying mechanoreceptors. (b) Hierarchical and interlocked microridge structured P(VDF-TrFE) and PDMS-based TESs. (c) Schematic illustration of gap distance change of TESs under vertical

pressure and theoretically calculated electric field distribution by COMSOL simulations depending on the width (w) and pitch (p) size of interlocked microridge arrays and planar structures. (d) Triboelectric voltage variations and pressure sensitivity following the size of interlocked microridge structured and planar films with the applied pressure. (e) Density of point contact between interlocked microridges under bending strain and coincident theoretically calculated electric field distribution by COMSOL simulations. The bending stress-induced (f) triboelectric voltage variations and bending sensitivity following the size of interlocked microridge structured and planar films with different bending angle.[37]

2.3 The proposed approach

Although piezoelectric and triboelectric sensors are relatively attractive for their high sensitivity and fast response time that are the key parameters for dynamic sensing, they are very susceptible to temperature and are not suitable for static force sensing. Besides, to obtain piezoelectric sensors' high sensibility, it is necessary to use inorganic materials which have a low flexibility. Instead, resistive-type sensors might demonstrate excellent flexibility and stretchability without a trade-off on its sensibility. However resistive-type sensors are dependent on the material used, which are not often reproducible which makes them not reliable enough for an electronic skin.

Unlike all those type of sensor, capacitive-type sensors are temperature-independent and can be shielded to reduce their susceptibility to electromagnetic waves. Intrinsically capacitive sensors do not rely on sensitive material development and are therefore comparatively easier to fabricate, exhibit fast response times and require lower power consumption [28]. Finally better suited for skin-like sensing capabilities, as they can be made sensitive to both static and dynamic force transduction [35]. Additionally, they can be readily integrated with energy conversion and storage devices such as supercapacitors or solar cells [29]. For these reasons, we chose to work on a capacitive based microstructured pressure and slip sensor, and in the next section, the sensor's design will be presented alongside the rationale behind its design.

Chapter 3. Design of the shear force sensor

The sensitivity of a sensor is its capability to detect and respond to the smallest change in response to an applied pressure. Numerous studies in the literature have reported sensors that demonstrate sensitivities equal to or better than that of human skin. Notably, both capacitive and resistive sensors offer improved detection thresholds compared to the skin. While the skin's detection threshold stands at 1 mN, those of capacitive and resistive sensors are respectively smaller than 0.05 mN and 0.08 mN. Furthermore, both capacitive and resistive sensors can achieve significantly enhanced response times. It can reach less than 10 ms and less than 20 ms for devices based on capacitance [38] and resistance [39], respectively. In comparison, the skin's response time is approximately 15 ms [19].

Typically, previous research has demonstrated sensors capable of detecting multidirectional forces but they all present a decrease in the sensitivity of sensors to shear when subjected to normal pressure [35], [40]. In the present study, the primary aim is to enhance the sensitivity of the pressure sensor to multidirectional forces such as shear and normal forces applied at the same time.

3.1 The proposed sensor's design

A change of capacitance will be observed either when the distance between the electrodes change, or when the overlapping area between the two electrodes is modified, or else when the relative permittivity of the dielectric will change [27]. Therefore, two solutions can be explored to tune the sensitivity of the flexible capacitor: the first one being the optimization of the conductivity of the conductive polymer composite; the second one being the refining of the mechanical and electrical properties of the dielectric layer.

The capacitive sensor consists in micropatterned electrodes arranged in 3D to act like combs as shown in the FIGURE 6**Error! Reference source not found.**. Compared to a flat electrode, under the same external pressure, the sensor made with a micropatterned electrode deforms significantly more due to the added compressibility, bringing the electrodes closer together, which further increases the capacitance change and sensitivity. The two layers are separated by a porous dielectric layer. All materials are based on PDMS. PDMS is made conductive for the electrode by mixing it with multiwalled carbon nanotubes (MWCNT). PDMS is made porous by using yeast evaporation method.

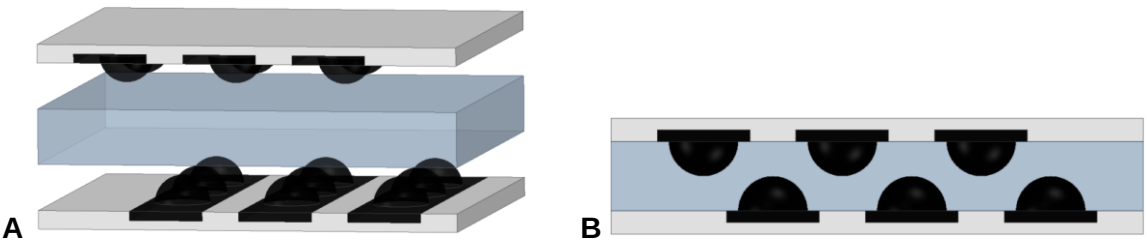

FIGURE 6 3D REPRESENTATION OF THE DESIGNED CAPACITIVE MICROSTRUCTURED PRESSURE AND SHEAR FORCE SENSOR. (A) Dismantled view of the sensor. (B) Cross-section view.

3.2 Improving conductivity of the polymer composite

For a flexible capacitive sensor, it is crucial to obtain a highly conductive material. This will allow to decrease the internal resistance of the sensors, hence decreasing the power consumption and improving the readout speed. In terms of readout electronics, increasing the conductivity of the electrodes will reduce the parasitic capacitance.

3.2.1 Choice of the conductive polymer composite

Rubbers such as polydimethylsiloxane are of great interest in the field of flexible sensors as they possess a great variety of properties such as mechanical flexibility and biocompatibility, although they are inherently insulating materials. On the other hand, metal suffers from compatibility issues with rubbers due to differences in their molecular structure [41]. Hence loading them with conductive nanofillers such as carbon black is known to increase their electrical conductivity [42]. Systematic studies have introduced the concept of percolation threshold that is the critical volume fraction for electron tunnelling to happen [43], [44].

Among polymers enhanced with nanofillers, carbon nanotubes (CNTs) based flexible polymer films are gaining in importance due to CNTs low percolation threshold at a lower weight percentage [45], [46]. In fact, because of their long tubular structure, they demonstrate high electrical conductivity ($10^6 - 10^7 S.m^{-1}$), mechanical flexibility, tensile strength of 63 Gpa [47] thermal stability and a high aspect ratio [48]. CNTs' high aspect ratio can be both an important advantage and a disadvantage. Its multiple active sites for redox reactions lead to faster electron transfer kinetics and therefore facilitates electron tunnelling. [49] Conversely, CNTs tend to aggregate as a result of van der Waals interactions supported by the high surface energy [42]. It is well established that a random and uniform dispersion of CNTs correlates to lower percolation threshold, and near that threshold, the conductivity increases drastically.

3.2.2 Preparation method of the conductive polymer composite

The preparation method of the polymer matrix have an important impact on the percolation threshold [50]–[52]. To be used in flexible and stretchable capacitive pressure sensors, the conductive polymer composite (CPC) needs to demonstrate good conductivity. Therefore, a good dispersion of the CNTs inside the polymer is necessary. The first challenge in the dispersion of the CNTs is to break the van der Waals interactions between the tubes from their initial aggregated state. Two methods have been previously employed to prepare the CNT-PDMS composites which are (1) dry blending using shear mixing [53], mechanical stirring, sonication, ball milling [54], and micro-bead milling [55] and (2) organic solvent methods [41], [56]–[58].

Although dry blending methods are safer and present less safety hazards, the physical shear stress is not enough to create sufficient local shear force. To achieve a homogeneous mixture inside the polymeric viscous matrix, higher stress should be applied, which leads the nanotubes to break into smaller tubes and their physical and electrical properties to change [41], [59]. Thus, shear mixing techniques such as drilling machine or sonication, aided by organic solvent dissolution or not, result in the significant increase of the percolation threshold and the decrease of the conductivity by more than 10 times, compromising too much the

nanocomposite for it to work as a sensing material [41]. Therefore, mechanical stirring with an organic polymer seems to be the best option for uniform dispersion of the nanofillers inside the polymer matrix.

3.2.3 Dispersion of the nanofillers inside the polymer matrix

Protocols involving dissolving CNT particles into solvent before mixing with PDMS have demonstrated reaching high levels of conductivity compared to the initial resistivity of the pure PDMS [60], [61]. The quality of the dispersion can be evaluated through the stability of the CNTs in their environment. The high quality dispersion is characterized by how small the aggregates remain and how long the dispersion persists.

In particular, Liu and Choi, 2012 [41] presented a standard characterisation protocol for dispersion of CNTs within polymers. They found that pristine MWCNTs were best dispersed in dimethylformamide (DMF), then chloroform and tetrahydrofuran (THF), and toluene was the worst case where apparent phase separation was leaving MWCNTs aggregates at the bottom of the vial.

In the case of PDMS, toluene was found to be the best solvent to dissolve PDMS base resin, followed by chloroform and THF that was found to own a high solubility of the PDMS base resin. Finally, DMF was found to react with PDMS base polymer, forming the gel-like substance upon mixing. Toluene having a poor dispersibility for MWCNTs and DMF reacting with PDMS base resin, chloroform and THF have been considered as a common solvent. Results showed that with the use of THF, the dispersion state was not stable, making chloroform the best candidate for both MWCNTs and the polymer matrix dissolution.

3.3 Improving the mechanical and electrical properties of the dielectric layer

Poly(dimethylsiloxane) (PDMS, commonly referred to as silicone elastomer) has emerged as a prominent silicon-based organic elastomer, with a rich history dating back to its first synthesis in the 1950s and subsequent adoption in academic research during the 1990s. PDMS is distinguished by its viscoelastic nature, biocompatibility, mechanical robustness, low glass transition temperature, cost-effectiveness, and moldability, rendering it highly suitable for practical applications. The presence of a silicon-oxygen-silicon (Si-O-Si) backbone imparts intriguing characteristics to PDMS, including flexibility, non-toxicity, non-flammability, thermal and electrical resistance, and low bulk density.

Furthermore, PDMS exhibits permeability to small, unreactive vapor and gas molecules like water and oxygen. Its surface properties are noteworthy, featuring low surface tension and hydrophobicity. It can undergo temporary hydrophilic modification through extensive hydroxyl group introduction via oxygen plasma treatment, although it eventually reverts to its inherent hydrophobic state due to chain migration. The surface of PDMS can be conveniently tailored through processes like oxygen plasma treatment, protein adsorption, or the conjugation of functional chemical groups.[62]

3.3.1 Improving the compressibility of the dielectric layer

Flexible capacitive sensors may be subject to high hysteresis due to the viscoelastic nature of rubber dielectrics, which represents one of the major disadvantages of flexible capacitive pressure sensors. To address this challenge, researchers have introduced air voids inside thin films of elastomers to alleviate problems associated with their viscoelastic behaviour [63]–[66]. Microengineering the dielectric layer presents many advantages, including an increase of the effective dielectric constant due to the collapse of the pores [64], therefore, higher sensitivity achievement, and a decrease of the Young's modulus and the viscoelastic properties of the elastomer [67].

Kim et al. studied the mechanical behaviour of porous PDMS for a capacitive pressure sensor using a FEA simulation tool [67]. They showed that the compressive modulus, that measures the resistance of the material to compression or changes in volume was found to be correlated with the volume of the air inside the pores. Initially, the presence of the air inside the pores provides compressibility to the porous material. With the increasing pressure, the compressive modulus was increasing as well, thus decreasing the sensitivity of the sensor. Increasing size of pores was giving increased sensitivity to the device, until the pores reach a certain size at which point an outward deflection was occurring. This deflection, referred to as buckling, was attributed to the Euler's critical load principle, according which the buckling phenomenon would occur [68]. The longer the column is, the lower is the critical force required for buckling to occur as shown in the FIGURE 7.

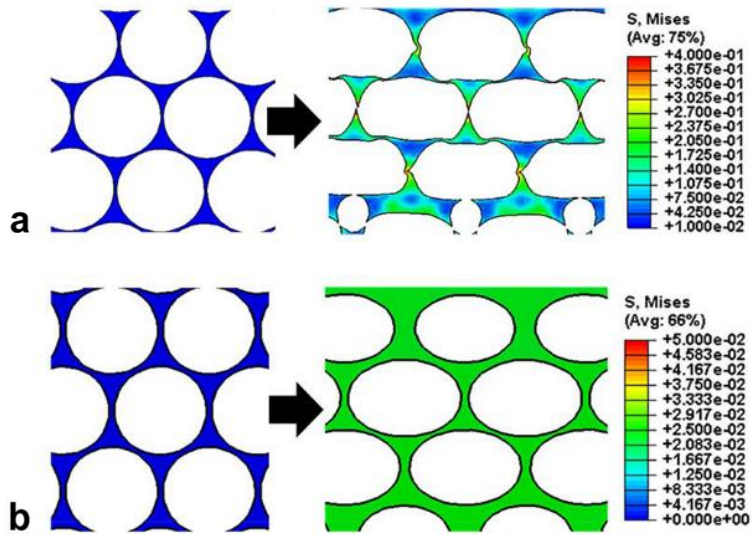

FIGURE 7 FEA SIMULATION OF STRAINED MICROSTRUCTURES WITH (A) 500 UM AND (B) 250 UM MICROPORES UNDER 30 KPA OF PRESSURE [67].

In 2020, Bao and Ruth have published a simple model assessing the importance of the form of the microstructures in the device's performances [64]. The dielectric layer is simply modelled as a series of springs and capacitors and using different structures, the model allows to assess how the mechanical and electrical properties of the sensor will be affected in response to a given applied pressure. As shown in the FIGURE 8, pyramids are the most suitable structure for enhancing performance. The stress is distributed nonuniformly across the pyramid microstructure and concentrates at its pointed tip. For low pressure, the tip of the

pyramid will compress more easily, and the micro-structured dielectric layer will stiffen for higher pressures, which will result in increased sensitivity but also increased dynamic range. Besides, they show that the sensitivity decreases as microstructures become more cuboid-like. Finally, this study shows that increasing distances between structures will increase the compressibility and the bendability of the sensor. Moreover, Deng et al. demonstrated that the base of the pyramid impact the sensitivity of the device. Making the base of the pyramids wider relative to its height decreases it.

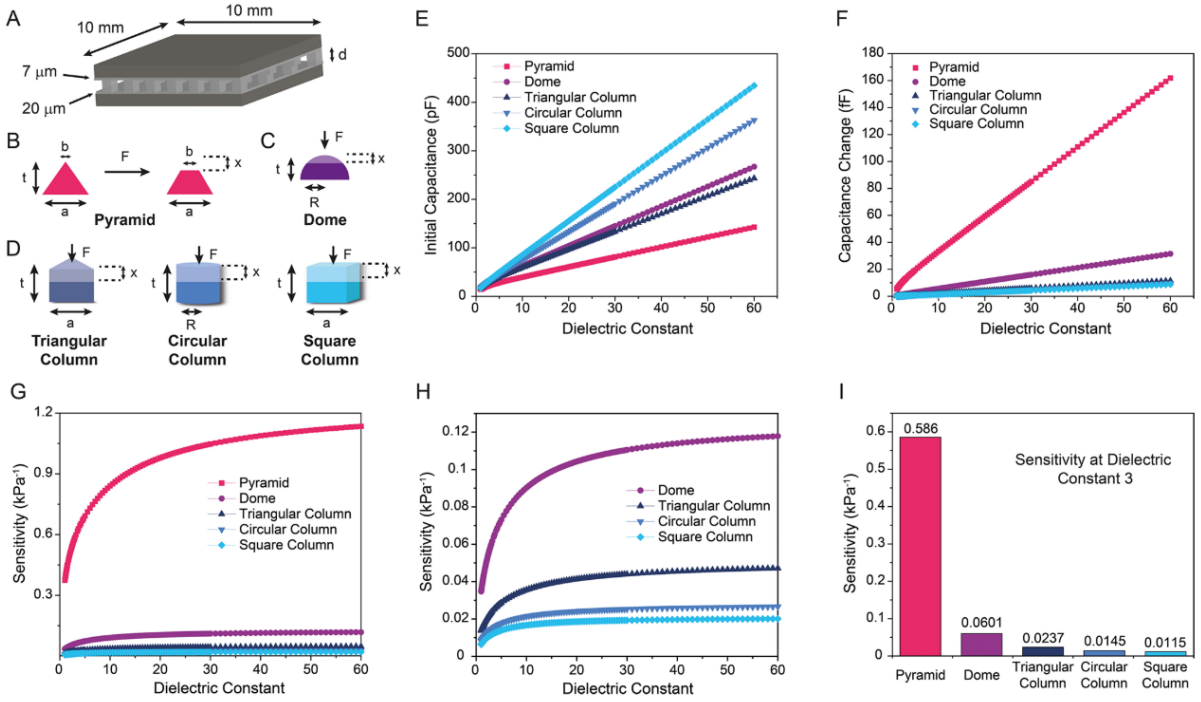

FIGURE 8 ANALYSIS OF THE EFFECT OF DIELECTRIC CONSTANT ON INITIAL CAPACITANCE, CAPACITANCE CHANGE, AND SENSITIVITY. (A) Dimensions of the parallel plate capacitive pressure sensor modelled in this work (not to scale) with a base layer of 20 μm and a lamination layer of 7 μm. (B) Labelled diagram of the pyramid microstructure with the dimensions represented in the model equations. (C) Labelled diagram of the dome microstructure with the dimensions represented in the model equations. As force is applied to the structure, the dome compresses. (D) Labelled diagram of the column microstructures with the dimensions represented in the model equations. As force is applied to the structure, the column compresses. (E) Initial capacitance increases linearly with dielectric constant for all five structures. For dielectric constant studies, the base length or diameter was 50 μm with an equivalent interstructural separation. (F) At 1 Pa of applied pressure, capacitance change increases linearly with increasing dielectric constant for all structures, but the pyramid structure has the highest slope. (G, H) Sensitivity has a logarithmic dependence on dielectric constant for all five structures, with the pyramid structure having the highest sensitivity for all values. (I) At a dielectric constant of 3, the sensitivity of the pyramid structures is the highest, followed by the dome with almost an order-of-magnitude lower sensitivity. [66]

3.3.2 Improving the dielectric constant

Polymers have usually higher dielectric constant than air. Therefore, introducing air in the polymer might lower its dielectric constant which is the absolute permittivity, but would increase its effective dielectric constant which is the relative permittivity. The dielectric constant is an intrinsic property of the material that has an impact on the initial capacitance of the sensor. However, in response to an applied pressure, as the pores begin to collapse, the ratio of air to elastomer decreases, and that leads to an increase of the effective dielectric constant. In this way, the sensitivity and the dynamic range of the sensor will be improved (FIGURE 9) [66], [67]. Furthermore, the effective dielectric constant increases in the presence of pores at low pressures, since the volume fraction of air to PDMS constantly changes. Such an additional effect further increases the sensitivity of our sensor at low pressures.

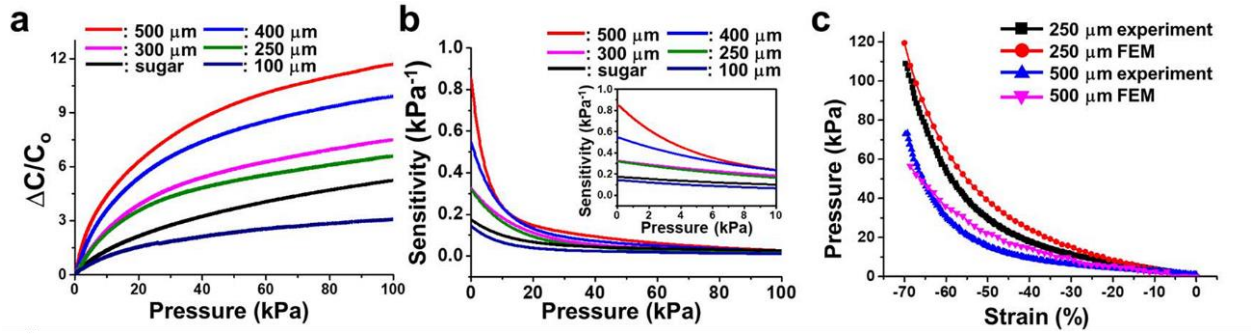

FIGURE 9 CHARACTERISTICS OF THE CAPACITIVE PRESSURE SENSOR FOR DIFFERENT MICROPORE SIZE. (a) Relative change of capacitance for increasing pressure. (b) Change of sensitivity for increasing pressure. The zoom-in shows the change of sensitivity for pressures below 10 kPa. (c) Experimental and simulated pressure curves for increasing strain percentages.

The decrease of the ratio air to elastomer in response to an applied pressure increases the also the dielectric constant [67]. The sensitivity being inversely proportional to the Young's modulus, larger pores will present a higher sensitivity in the low-pressure region with an abrupt decrease of sensitivity in the high-pressure region (FIGURE 9B).

3.3.3 Overcoming the challenge of micropatterning the dielectric layer

According to the desired functions, an appropriate fabrication method should be adopted to produce PDMS sponges with the requisite structural characteristics, including pore geometry, pore size, pore distribution, and closed/open porous frameworks. Not every fabrication method can meet the needs of every envisaged application. In addition to the physical structure of the pores, the functionalities of PDMS sponges and their pore surfaces are also important.

A common technique for PDMS sponge fabrication involves using solid templates as porogens. These templates, such as salt crystals and sugar cubes, can be dissolved or removed, leaving behind a PDMS structure with interconnected voids. The simplicity of this method, which relies on water as a leaching agent, has led to its widespread use. Yu et al. introduced a modified approach using citric acid monohydrate and ethanol, where the solvent efficiently wets PDMS and dissolves the template.

PDMS sponges using emulsion templates are made by polymerizing the continuous emulsion phase. Pore formation relies on emulsion droplets. The technique offers controlled interconnected or separate pores with a narrow size distribution, suitable for upscaling. However, the surfactant used can impact the polymer's post-synthesis performance, and removing it is often challenging. Still, this method is frequently used to make 3D porous polymers for applications like tissue engineering, separation, and water retention.

Advances in the manufacture of additives have drawn much attention so far this century and have resulted in numerous improved approaches for 3D printing using PDMS. However, the direct 3D printing of PDMS to form complex structures is still challenging, owing to the low elastic modulus of the liquid prepolymer.

Porous materials are produced through phase separation methods, including thermally induced phase separation (TIPS), nonsolvent-induced phase separation (NIPS), vapor-induced phase separation (VIPS), and solvent evaporation-induced phase separation (EIPS). These methods rely on solvent evaporation to transition from a single phase to a two-phase region, creating porous structures as the solvent is removed. The resulting fibers exhibit porosity after complete solvent removal.

Although the above techniques have proven an efficient way of forming pores inside the polymer, they all use solvents. Use of solvent is highly unrecommended in our case, as it can lead to the denaturation of the conductive property of the MWCNT-PDMS polymer composite. Gas foaming is a known technique for producing polymer foams used in various applications, including sealants, shock absorbers, and insulators. However, it has limitations in controlling pore size and connectivity. Pores can be generated through chemical, physical, or biological means. To address issues related to water content affecting sponge properties, Brook et al. introduced the Piers-Rubinsztajn reaction, producing well-defined silicone structures with gaseous by-products as blowing agents, enabling rapid, high-yield fabrication at room temperature.

An interesting approach for the rapid and easy fabrication of the porous polymer is the use of the very commonly used yeast (*Saccharomyces Cerevisiae*) in baking industry. *Saccharomyces Cerevisiae* is a unicellular micro-organism that is dying by autolysis in response to an increase in temperature above $43℃$. The autolysis is referred to the process in which a yeast cell is digesting itself after death occurs. Following cell death, enzymes are released that act to degrade cellular constituents. Those constituents are mostly gaseous due to the fermentation capability of yeast [69].

Chapter 4. Fabrication of the sensor

In this part, a systematic study was conducted on the impedance, conductivity and Young's modulus of the conductive polymer composite (CPC) using an innovative technique to disperse the CNTs inside the polymer. The good dispersion of the CNTs has been evaluated by proportionally increasing the size of the samples and comparing their electrical conductivity over their surface.

4.1 Methods

4.1.1 Materials

The MWCNTS used in the following experiments came from Nanografi Turkey (purity >90%, outside diameter: 50-80 nm, inside diameter: 5-15 nm, length: 10-30 µm). The silicon rubber (polydimethylsiloxane (PDMS), Sylgard 184) used as the polymer matrix was purchased from DOW Corning Inc., Wiesbaden, Germany, including the base resin (part A) and the curing agent (part B) to be mixed in a ratio of 10:1.

SLA printer (Formlabs, Form 3+) was used to print the moulds. Moulds are printer in resin (Formlabs, Clear Resin V4 1L) which is a UV sensitive material. This stereolithography 3D printer uses a light source to cure the liquid resin directly on the build platform [70]. The resolution of the print is determined by the z-axis layer height which can be varied between 25 and 300 microns. For those reasons, the SLA printers are capable to produce high resolution and accuracy, isotropic, smooth surface parts.

4.1.2 Capacitive-based microstructured shear force sensor assembly overview

The different steps are represented in the FIGURE 10:

1. The CNT/PDMS is poured in the first mould in order to obtain the microstructured electrodes.
2. The electrodes are peeled off and placed in a second mould.
3. Pure PDMS is coated on top of the electrodes.
4. The substrate is peeled off and placed in a third mould.
5. PDMS/yeast mixture is poured on top of the substrate and half-cured to obtain the porous dielectric.

The five first steps are repeated twice, and the two halves are combined before finishing curing.

All those steps rely on finding a way to develop a robust and reproducible mould fabrication. In fact, number of microstructures devices are based on the fabrication of moulds using photolithography technique. However, this technique is very expensive, thus limiting the ability to test different geometries easily. Here, I propose to 3D print the moulds in resin with an SLA printer.

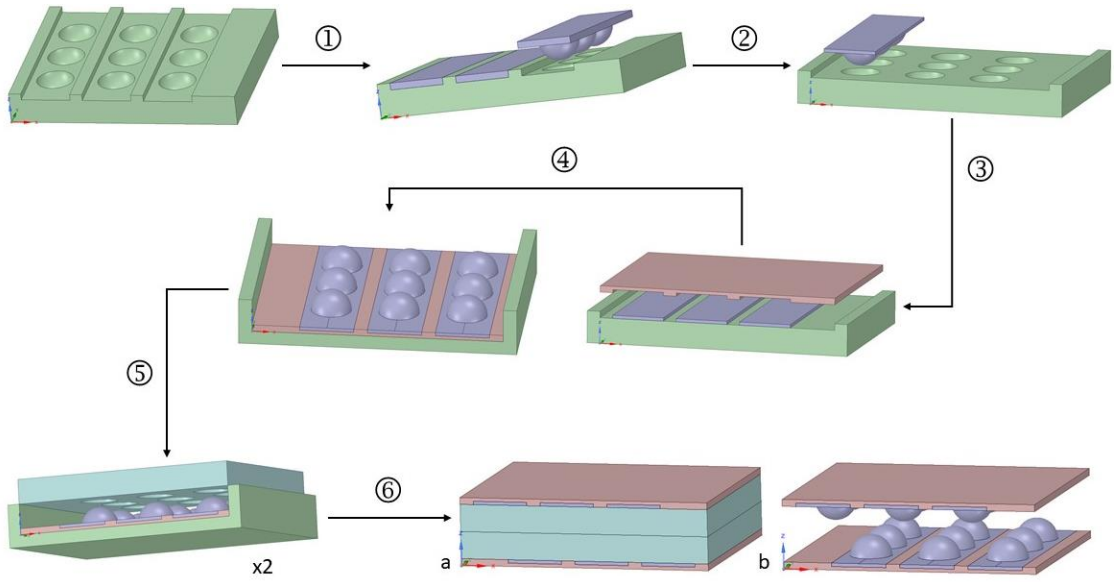

FIGURE 10 THE STEPS INVOLVED IN THE FABRICATION OF THE SENSOR. At the ultimate step, (a) represents the view with the dielectric layer, (b) represents the view without the dielectric layer. Both are the same device.

4.1.3 Preparation of MWCNT-PDMS composite

The protocol followed for this step is. MWCNT is dispersed inside chloroform, then the solution is added to the PDMS base resin. Different concentration of MWCNT can be considered. The mixture is then placed under magnetic bar stirring for 1h to allow proper mixing of the MWCNTs with the PDMS base resin. After 1h, the white cap of the beaker is removed and the solution is maintained on the hot plate at 64°C under continuous stirring overnight to remove all the solvent. The complete evaporation of the solvent is ensured by weighing the preparation before addition of chloroform and after. Finally, the curing agent is added in the weight ratio of 10:1 (base: curing agent).

4.1.4 Preparation of the porous PDMS

PDMS was initially proposed as an antifoam for controlling foam formation in wine fermentation and in brewery fermentation. Vernon and Rose have shown that PDMS was absorbed by *Saccharomyces Cerevisiae* when it was dispersed in an aqueous emulsion that contained emulsifiers and cellulose-based thickeners. In their study, concentration of PDMS was not a factor for the absorption velocity, and the total time to reach saturation was about 2 to 4 hours [71]. This interesting property added to autolysis of the cells in response to an increase in temperature has been proven to be an efficient single step process for fabrication of porous elastomers [72].

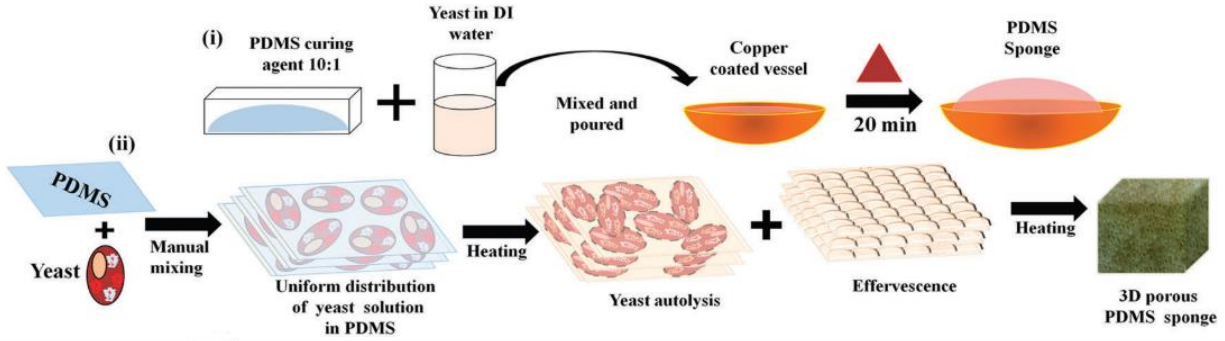

FIGURE 11 FABRICATION PROCESS OF THE POROUS PDMS USING YEAST [72]

The protocol followed for this step is the protocol proposed by Parameswaran & Gupta, 2018 [72]. A yeast solution is prepared by diluting dry yeast inside DI water. Different concentration of yeast can be considered. Then the solution is added to the PDMS base resin and mixed thoroughly. Finally, the curing agent is added in the weight ratio of 10:1 (base: curing agent). Particular attention should be brought on the rapidity of those steps as PDMS was shown to be absorbed by *Saccharomyces Cerevisiae* when it was dispersed in an aqueous emulsion that contained emulsifiers and cellulose-based thickeners. Besides, concentration of PDMS was not a factor for the absorption velocity, and the total time to reach saturation was about 2 to 4 hours [71]. Finally, the mixture is poured on the electrodes and put in the oven for curing for 2 hours at 70°C.

In this paper [72], different sizes of pores are obtained, from $10\ \mu m$ up to $500\ \mu m$. According to Parameswaran & Gupta, it is expected that slow curing of the mixture would lead to the formation of the small pores. With higher curing temperatures, effervescence accumulate and doesn't have time to dissipate, so we observe formation of larger pores. Moreover, use of surfactant invert the foam's hydrophobicity to make it hydrophilic [73]. This allows the permittivity to drop and make it suitable for capacitive sensing. The challenge to address here concern concentration of the heat on the samples and the dissipation of water after evaporation from the PDMS. In the case of curing on a hot plate, water is directly dissipated in the air. In the case of curing inside an oven, heat is dispersed in a determined volume, and air is not spontaneously dissipated.

4.1.5 Measurement of electrical properties of MWCNT-PDMS

In the absence of scanning electron microscopy (SEM) or transmission electron microscopy (TEM), the investigation of the electrical properties of the CPC, electrical impedance spectroscopy (EIS) has shown to be valuable tool as the AC conductivity is used to characterise the frequency responses of MWCNT-PMDS near the percolation threshold [42]. As seen in the **FIGURE 12**, the percolation theories are commonly used to explain the insulator-to-conductor transitions in conductive polymer composites [74].

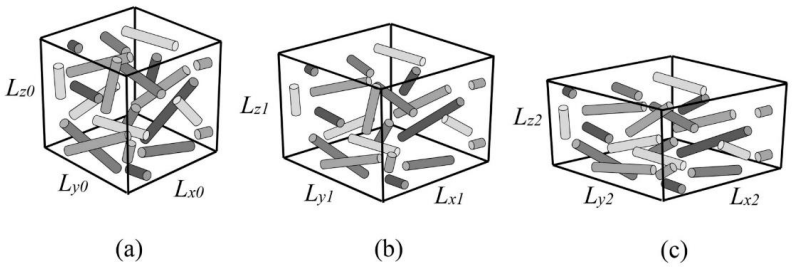

FIGURE 12 DISTRIBUTION OF CARBON NANOTUBES INSIDE THE POLYMER MATRIX. The image shows from (a) to (b) that the distribution is function of length, width and thickness of the polymer [42].

It is possible to model the network of carbon nanotubes inside the polymer matrix assuming a simple linear model in which a set of parallel RC-circuits connected in series represents the network of carbon nanotubes. In this model, each junction has an impedance given by:

$$Z = \frac{R_i}{1 + j\omega R_i C_i}$$

where the resistance R_i and the capacitance C_i correspond to the ith element. The total impedance of the equivalent circuit is then the sum of the all individual impedance of each junction. Assuming that there are N number of series connected elements, and if R_s is the series resistance associated with the contact between surfaces and the bulk, the impedance becomes:

$$Z = R_s + \sum_{i=1}^{N} \frac{R_i}{1 + j\omega R_i C_i}$$

This equation shows that the resistance R_i has a significantly larger range than the capacitance C_i. In fact, as the filler fraction increases, the capacitance may change by three orders of magnitude, whereas the resistance may increase six orders of magnitude. The MWCNTs are assumed to be randomly aligned in the polymer matrix, therefore the number of possible conducting paths is large, and the more randomly they are aligned, the larger is the number of possible paths.

4.2 Results and discussion

4.2.1 Impedance measurements of MWCNT-PDMS

To test the homogeneity of the dispersion method, instead of using qualitative SEM imaging, a quantitative method has been developed. The assumption here is that if the dispersion of the conductive nanofillers is homogeneous, then increasing the surface area of the CPC won't affect the conductivity per area of the CPC. Therefore, in the first setup **FIGURE 13A,** from left to right, the overall area of the polymer composite has been increased two times, we call them square 4×4, square 2×2 and square 1×1; in the second setup **FIGURE 13B**, the length of the polymer composite between the two electrodes has been increased, we call them length 4×1, length 2×1 and length 1×1; in the third setup **FIGURE 13C**, the width of the electrode has been increased, we call them width 1×1, width 1×2 and width 1×4.

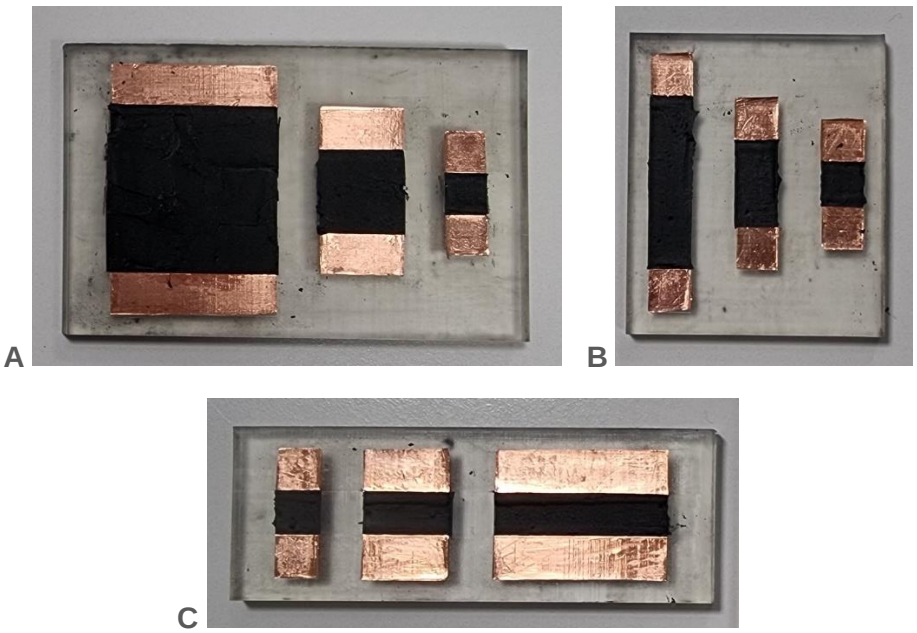

FIGURE 13 PROPOSED SET-UP FOR MEASURING CONDUCTIVITY OF THE FABRICATED CPC AND THE HOMOGENEITY OF THE NANOFILLERS DISPERSION. The conductivity has been evaluated with increasing length, increasing width and increasing surface area of the polymer. For each sample, the value of the length or of the width or of both of them has been doubled. (A) square study (4×4), (2×2) and (1×1). (B) length study (4×1), (2×1) and (1×1). (C) width study (1×4), (1×2) and (1×1)

A low conductivity of the electrodes in a capacitor implicate a reduced initial capacitance, a slower response time, a non-linear behaviour and an increase in signal loss. In terms, it leads to a higher noise levels and a reduced sensitivity. Therefore, to be sure that the conductive polymer composite is conductive enough to obtain a good sensitivity from the device, the MWCNT-PDMS should meet the condition of a phase angle equal to 0°.

The impedance for each condition has been measured; the phase plots and the bode diagrams are reported in the **FIGURE 14**. The 0° phase angle condition is met in the **FIGURE**

14A for low frequency range, from 0.1 to 1 kHz, and in the FIGURE 14B up to 80 kHz. Besides, the bode diagram in the FIGURE 14C shows a high resistance at 1 kHz frequency, varying between $1.78 \times 10^3\ \Omega$ and $4.55 \times 10^4\ \Omega$ which translates to high voltage input in order to get a response from the capacitor, whereas in the FIGURE 14D, the overall resistance is much lower, varying between $6.37 \times 10^1\ \Omega$ and $1.32 \times 10^3\ \Omega$.

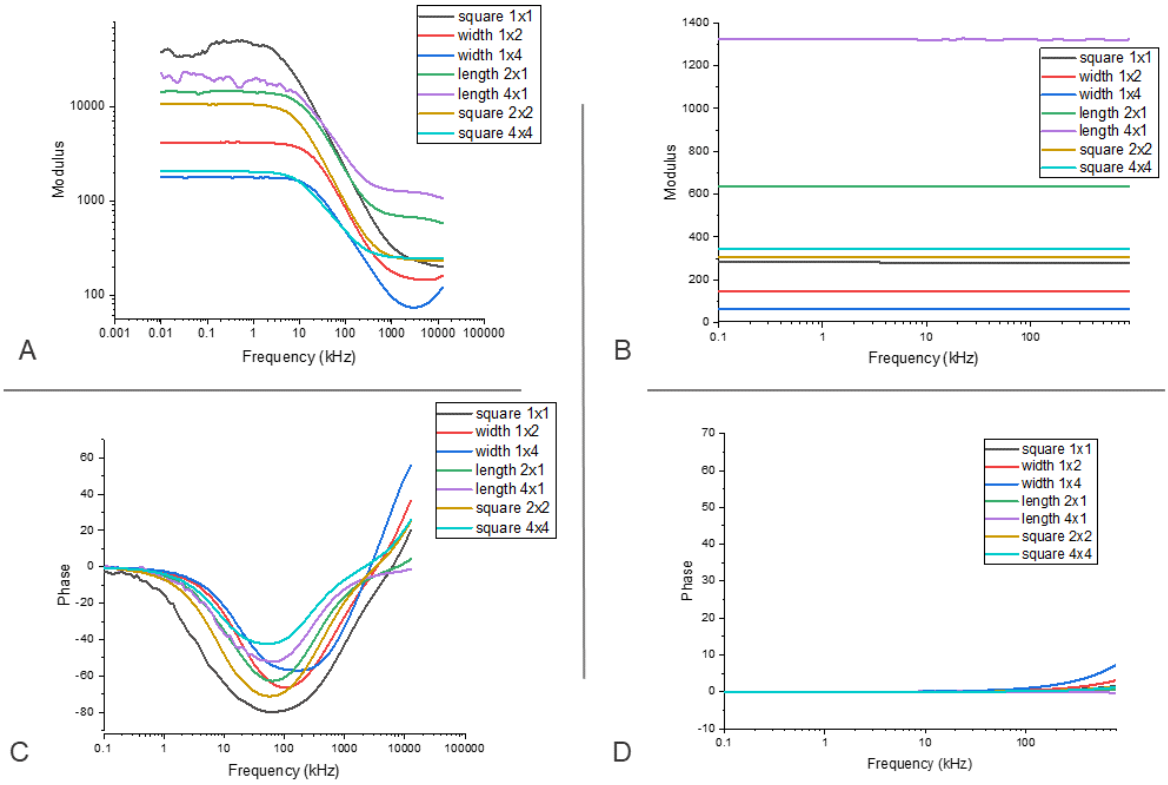

FIGURE 14 A & B PHASE PLOT OF MWCNT-PDMS **POLYMER COMPOSITE DEPOSITED ON (A) COPPER TAPE AND (B) SILVER PASTE. C & D BODE DIAGRAM OF** MWCNT-PDMS **POLYMER COMPOSITE DEPOSITED ON (C) COPPER TAPE AND (D) SILVER PASTE.**

Here, we show that the contact between the conductive polymer composite and the electrode plays a significant role in the ability to detect a signal from the device. In fact, while the adhesion of the mould made with resin and the copper tape was poor, the adhesion of the silver paste to the resin was much stronger. Therefore, during the deposition and curing of MWCNT-PDMS on copper tape, as copper tape was detaching from the mould, the contact area would vary, adding some contact resistance to the measurements. In contrast, it is clear that with the silver paste, the contact area was much better for all the samples, as they demonstrate a certain uniformity: MWCNT-PDMS polymer samples were all in-phase over the larger part of the frequency range. The variation of the resistance in the bode diagram can therefore be attributed to the dispersion of the carbon nanotubes inside the polymer matrix.

4.2.2 IV measurements of MWCNT-PDMS

IV curves of the same samples have been measured from $-20V$ to $+20V$ and reported in the FIGURE 15. Here, the conductivity has been calculated based on the Ohm's law where the resistivity can be calculated from the electrical resistance (R) of the material. The resistance

is directly proportional to its resistivity (ρ) and length (L), and inversely proportional to its cross-sectional area (A) and is expressed in $\Omega.m$. The resistivity is given by:

$$\rho = \frac{R \times A}{L}$$

In other words, the resistance increases with the increasing length of the material, the decreasing cross-sectional area of the material and an increasing resistivity of the material. The conductivity (σ) of a material, though, is inversely proportional to the resistivity and is typically expressed in $S.m^{-1}$. The conductivity is given by:

$$\sigma = \frac{1}{\rho}$$

The conductivity curves over the voltage show a homogeneity in the material properties.

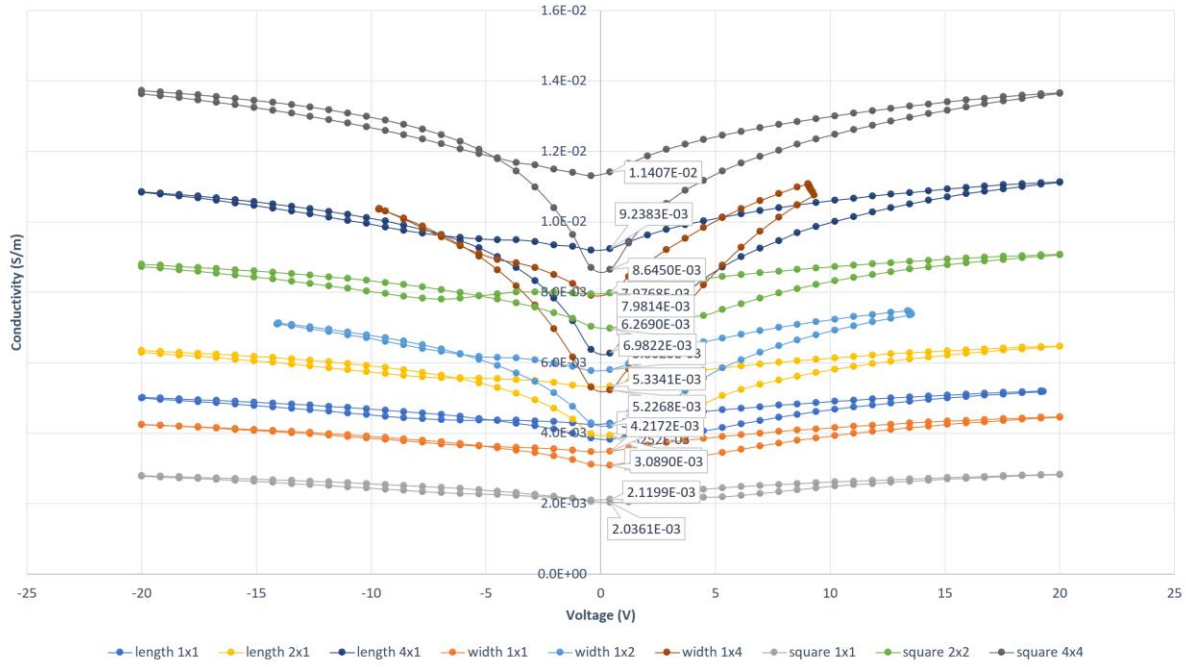

FIGURE 15 MEASUREMENTS OF THE CONDUCTIVITY OF THE PDMS-MWCNT POLYMER COMPOSITE IN BETWEEN THE RANGE OF -20V AND 20V

TABLE 3 gives a comparison between the calculated resistivity from impedance measurements and I/V measurements of the samples with the silver paste. This table demonstrate that with higher voltage input, it is possible to significantly decrease the resistivity, and therefore increase the conductivity of the MWCNT-PDMS polymer composite. Besides, this table shows a better uniformity in the measured conductivities among the different samples, showing a uniform dispersion of the CNTs inside the polymer matrix. However, the tunnelling effect with high voltage cannot be excluded. We previously assumed that the CPC could be modelled by an equivalent circuit of randomly distributed resistors and capacitors. Higher voltage would charge the capacitors to saturation, leaving only the resistors. CNTs being known as excellent conductors, the resistivity of those resistors that is measured results in low resistivity.

Sample	Length (mm)	Width (mm)	Thickness (mm)	Area of contact (mm²)	ρ from Z/f measurements ($\Omega.mm^{-1}$)	ρ from I/V measurements ($\Omega.mm^{-1}$)
1	10	10	1	10	2.84×10^2	2.15×10^2
2	10	20	1	20	2.93×10^2	1.53×10^2
3	10	40	1	40	4.00×10^3	1.04×10^2
4	20	10	1	10	3.21×10^2	1.74×10^2
5	20	20	1	20	3.26×10^2	1.21×10^2
6	40	10	1	10	3.33×10^2	1.02×10^2
7	40	40	1	40	3.45×10^2	8.06×10^1

TABLE 3 COMPARISON OF CALCULATED RESISTIVITY FROM Z/F MEASUREMENTS AND I/V MEASUREMENTS

Chapter 5. Conclusion

5.1 Fabrication of the conductive polymer composite

In this work, we have shown the critical role that the contact resistance play into the measurement of the conductivity of the conductive polymer composite. A better contact leads to lower voltage input and a lower working frequency range for the CPC to be highly conductive. This allows to decrease the internal resistance of the sensors, hence decreasing the power consumption and improving the readout speed. In terms of readout electronics, an increased conductivity of the electrodes reduces the parasitic capacitance. However, as seen in this work, the CPC is directly cured on non stretchable, although flexible, copper tape. Use of silver paste was more promising, but silver paste has a poor adhesion to PDMS. Therefore, future work will concentrate on the integration of conductive wire on soft substrate in order to reduce to the minimum the contact resistance while also keeping the flexibility and stretchability properties of the device.

5.2 Preliminary results of the porous PDMS fabrication

The major issue encountered during the fabrication of the porous PDMS was the curing of the PDMS after pouring inside the printed mould on top of the flexible electrodes. Several hypotheses have been proposed to explain this issue.

First of all, if the addition of the curing agent and the curing of the PDMS was occurring too long after mixing the PDMS base resin with the yeast solution, then the curing wasn't happening at all. This is supposed to be due to the fact that yeasts are absorbing PDMS as seen in [71]. However, this hypothesis is not confirmed; therefore, we cannot make a definitive statement based on that. In fact, higher concentrations of yeast was preventing curing of the porous polymer.

Another hypothesis concerns the cross-linking of polysiloxane. In fact, the second step of the cross-linking reaction requires some platinum during 2 hours at 75°C. It cannot be excluded that one or more byproduct of the yeast autolysis reacts with the platinum contained inside the curing agent. In order to test this hypothesis, four samples have been prepared in a Petri dish; (i) containing pure PDMS, (ii) containing PDMS mixed with DI water, (iii) containing PDMS mixed with dry yeast, and (iv) containing PDMS mixed with yeast solution. Surprisingly, all samples cured entirely.

The same experiment have been repeated by printing moulds in the size equal or similar to the Petri dish. In this case, all samples cured, except the PDMS mixed with the yeast solution. Therefore, it has been established that the printed mould was somehow preventing the crosslinking of the PDMS. The only difference between the printed mould and the Petri dish is that the printed mould has been cleaned with a solvent after printing and cured under UV. To mimic this difference, the experiment has been repeated by pre-treating the Petri dish with a solvent and drying in the oven. It has been observed that in that case, the crosslinking was not happening again. The final hypothesis is that after printing, the solvent needs to be

removed completely because it might interfere with the crosslinking of the PDMS mixed with yeast solution.

Different techniques will be further explored during the last year of my research to achieve a reproducible porous PDMS fabrication protocol. Finally, the assembly of the sensor depends greatly on our ability to obtain a porous dielectric layer.

Chapter 6. Bibliography

[1] W. H. Warren, “The dynamics of perception and action,” *Psychol. Rev.*, vol. 113, no. 2, pp. 358–389, 2006, doi: 10.1037/0033-295X.113.2.358.

[2] R. S. Johansson and K. J. Cole, “Sensory-motor coordination during grasping and manipulative actions.,” *Curr. Opin. Neurobiol.*, vol. 2, no. 6, pp. 815–23, Dec. 1992, doi: 10.1016/0959-4388(92)90139-c.

[3] R. S. Johansson, “Sensory Control of Dexterous Manipulation in Humans,” *Hand Brain*, pp. 381–414, 1996, doi: 10.1016/b978-012759440-8/50025-6.

[4] R. S. Johansson and J. R. Flanagan, “Coding and use of tactile signals from the fingertips in object manipulation tasks,” *Nature Reviews Neuroscience*, vol. 10, no. 5. Nature Publishing Group, pp. 345–359, May 2009, doi: 10.1038/nrn2621.

[5] I. Nisky, F. A. Mussa-Ivaldi, and A. Karniel, “A regression and boundary-crossing-based model for the perception of delayed stiffness,” *IEEE Trans. Haptics*, vol. 1, no. 2, pp. 73–83, 2008, doi: 10.1109/TOH.2008.17.

[6] L. A. Jones and I. W. Hunter, “A perceptual analysis of viscosity.,” *Exp. brain Res.*, vol. 94, no. 2, pp. 343–51, 1993, doi: 10.1007/BF00230304.

[7] M. Kuschel, M. Di Luca, M. Buss, and R. L. Klatzky, “Combination and integration in the perception of visual-haptic compliance information,” *IEEE Trans. Haptics*, vol. 3, no. 4, pp. 234–244, 2010, doi: 10.1109/TOH.2010.9.

[8] R. S. Johansson, “Tactile sensibility in the human hand: Receptive field characteristics of mechanoreceptive units in the glabrous skin area,” *J. Physiol.*, vol. 281, pp. 101–123, 1978, doi: 10.1113/jphysiol.1978.sp012411.

[9] R. S. Johansson and A. B. Vallbo, “Tactile sensibility in the human hand: relative and absolute densities of four types of mechanoreceptive units in glabrous skin.,” *J. Physiol.*, vol. 286, pp. 283–300, Jan. 1979, doi: 10.1113/jphysiol.1979.sp012619.

[10] R. S. Johansson and A. B. Vallbo, “Detection of tactile stimuli. Thresholds of afferent units related to psychophysical thresholds in the human hand.,” *J. Physiol.*, vol. 297, no. 1, pp. 405–422, Dec. 1979, doi: 10.1113/jphysiol.1979.sp013048.

[11] R. S. Johansson and Å. B. Vallbo, “Spatial properties of the population of mechanoreceptive units in the glabrous skin of the human hand,” *Brain Res.*, vol. 184, no. 2, pp. 353–366, 1980, doi: 10.1016/0006-8993(80)90804-5.

[12] R. S. Johansson and R. H. Lamotte, “Tactile detection thresholds for a single asperity on an otherwise smooth surface,” *Somatosens. Mot. Res.*, vol. 1, no. 1, pp. 21–31, 1983, doi: 10.3109/07367228309144538.

[13] R. S. Johansson and G. Westling, “Roles of glabrous skin receptors and sensorimotor memory in automatic control of precision grip when lifting rougher or more slippery objects.,” *Exp. brain Res.*, vol. 56, no. 3, pp. 550–64, 1984, doi: 10.1007/BF00237997.

[14] J. Gerardo Rocha and S. Lanceros-Mendez, *Sensors: Focus on Tactile Force and Stress Sensors*. 2008.

[15] R. Dahiya, G. Metta, M. Valle, and G. Sandini, “Tactile Sensing—From Humans to

Humanoids," *IEEE Trans. Robot.*, vol. 26, no. 1, pp. 1–20, Feb. 2010, doi: 10.1109/TRO.2009.2033627.

[16] M. L. Hammock, A. Chortos, B. C. K. Tee, J. B. H. Tok, and Z. Bao, "25th anniversary article: The evolution of electronic skin (E-Skin): A brief history, design considerations, and recent progress," *Adv. Mater.*, vol. 25, no. 42, pp. 5997–6038, 2013, doi: 10.1002/adma.201302240.

[17] W. Ge and P. S. Khalsa, "Encoding of compressive stress during indentation by slowly adapting type I mechanoreceptors in rat hairy skin," *J. Neurophysiol.*, vol. 87, no. 4, pp. 1686–1693, 2002, doi: 10.1152/jn.00414.2001.

[18] P. R. Burgess, J. Mei, R. P. Tuckett, K. W. Horch, C. M. Ballinger, and D. A. Poulos, "The neural signal for skin indentation depth. I. Changing indentations.," *J. Neurosci.*, vol. 3, no. 8, pp. 1572–85, Aug. 1983, doi: 10.1523/JNEUROSCI.03-08-01572.1983.

[19] A. Chortos, J. Liu, and Z. Bao, "Pursuing prosthetic electronic skin," *Nat. Mater.*, vol. 15, no. 9, pp. 937–950, 2016, doi: 10.1038/nmat4671.

[20] E. R. Kandel, J. H. Schwartz, T. M. Jessel, S. A. Siegelbaum, and A. J. Hudspeth, "Touch," in *Principles of Neural Science*, Fifth Edit., 2013, pp. 1689–1699.

[21] R. Dahiya, "E-Skin: From Humanoids to Humans [Point of View]," *Proc. IEEE*, vol. 107, no. 2, pp. 247–252, Feb. 2019, doi: 10.1109/JPROC.2018.2890729.

[22] W. Navaraj, C. Smith, and R. Dahiya, "E-skin and wearable systems for health care," in *Wearable Bioelectronics*, Elsevier, 2019, pp. 133–178.

[23] M. Soni and R. Dahiya, "Soft Eskin: Distributed touch sensing with harmonized energy and computing," *Philos. Trans. R. Soc. A Math. Phys. Eng. Sci.*, vol. 378, no. 2164, 2020, doi: 10.1098/rsta.2019.0156.

[24] J. C. Yeo, J. Yu, Z. M. Koh, Z. Wang, and C. T. Lim, "Wearable tactile sensor based on flexible microfluidics," *Lab Chip*, vol. 16, no. 17, pp. 3244–3250, 2016, doi: 10.1039/C6LC00579A.

[25] J. Park *et al.*, "Tactile-direction-sensitive and stretchable electronic skins based on human-skin-inspired interlocked microstructures," *ACS Nano*, vol. 8, no. 12, pp. 12020–12029, 2014, doi: 10.1021/nn505953t.

[26] R. Puers, "Capacitive sensors: When and how to use them," *Sensors Actuators A. Phys.*, vol. 37–38, no. C, pp. 93–105, 1993, doi: 10.1016/0924-4247(93)80019-D.

[27] R. B. Mishra, N. El-Atab, A. M. Hussain, and M. M. Hussain, "Recent Progress on Flexible Capacitive Pressure Sensors: From Design and Materials to Applications," *Adv. Mater. Technol.*, vol. 6, no. 4, pp. 1–34, 2021, doi: 10.1002/admt.202001023.

[28] N. Khalili, X. Shen, and H. E. Naguib, "An interlocked flexible piezoresistive sensor with 3D micropyramidal structures for electronic skin applications," *Soft Matter*, vol. 14, no. 33, pp. 6912–6920, 2018, doi: 10.1039/c8sm00897c.

[29] C. Cao, Y. Chu, Y. Zhou, C. Zhang, and S. Qu, "Recent Advances in Stretchable Supercapacitors Enabled by Low-Dimensional Nanomaterials," *Small*, vol. 14, no. 52, pp. 1–26, 2018, doi: 10.1002/smll.201803976.

[30] T. Yamada *et al.*, "A stretchable carbon nanotube strain sensor for human-motion detection," *Nat. Nanotechnol.*, vol. 6, no. 5, pp. 296–301, 2011, doi: 10.1038/nnano.2011.36.

[31] W. Hu, X. Niu, R. Zhao, and Q. Pei, “Elastomeric transparent capacitive sensors based on an interpenetrating composite of silver nanowires and polyurethane,” *Appl. Phys. Lett.*, vol. 102, no. 8, 2013, doi: 10.1063/1.4794143.

[32] D. J. Lipomi *et al.*, “Skin-like pressure and strain sensors based on transparent elastic films of carbon nanotubes,” *Nat. Nanotechnol.*, vol. 6, no. 12, pp. 788–792, Dec. 2011, doi: 10.1038/nnano.2011.184.

[33] F. Xu and Y. Zhu, “Highly conductive and stretchable silver nanowire conductors,” *Adv. Mater.*, vol. 24, no. 37, pp. 5117–5122, 2012, doi: 10.1002/adma.201201886.

[34] X. Wang, T. Li, J. Adams, and J. Yang, “Transparent, stretchable, carbon-nanotube-inlaid conductors enabled by standard replication technology for capacitive pressure, strain and touch sensors,” *J. Mater. Chem. A*, vol. 1, no. 11, pp. 3580–3586, 2013, doi: 10.1039/c3ta00079f.

[35] C. M. Boutry *et al.*, “A hierarchically patterned, bioinspired e-skin able to detect the direction of applied pressure for robotics.,” *Sci. Robot.*, vol. 3, no. 24, pp. 1–10, Nov. 2018, doi: 10.1126/scirobotics.aau6914.

[36] Z. L. Wang, J. Chen, and L. Lin, “Progress in triboelectric nanogenerators as a new energy technology and self-powered sensors,” *Energy Environ. Sci.*, vol. 8, no. 8, pp. 2250–2282, 2015, doi: 10.1039/c5ee01532d.

[37] M. Ha *et al.*, “Skin-Inspired Hierarchical Polymer Architectures with Gradient Stiffness for Spacer-Free, Ultrathin, and Highly Sensitive Triboelectric Sensors,” *ACS Nano*, vol. 12, no. 4, pp. 3964–3974, 2018, doi: 10.1021/acsnano.8b01557.

[38] G. Schwartz *et al.*, “Flexible polymer transistors with high pressure sensitivity for application in electronic skin and health monitoring,” *Nat. Commun.*, vol. 4, no. May, 2013, doi: 10.1038/ncomms2832.

[39] S. Lee *et al.*, “A transparent bending-insensitive pressure sensor,” *Nat. Nanotechnol.*, vol. 11, no. 5, pp. 472–478, 2016, doi: 10.1038/nnano.2015.324.

[40] J. Park *et al.*, “Giant tunneling piezoresistance of composite elastomers with interlocked microdome arrays for ultrasensitive and multimodal electronic skins,” *ACS Nano*, vol. 8, no. 5, pp. 4689–4697, 2014, doi: 10.1021/nn500441k.

[41] C. X. Liu and J. W. Choi, “Improved dispersion of carbon nanotubes in polymers at high concentrations,” *Nanomaterials*, vol. 2, no. 4, pp. 329–347, 2012, doi: 10.3390/nano2040329.

[42] L. E. Helseth, “Electrical impedance spectroscopy of multiwall carbon nanotube-PDMS composites under compression,” *Mater. Res. Express*, vol. 5, no. 10, 2018, doi: 10.1088/2053-1591/aada3c.

[43] L. K. . Van Beek and B. I. C. . Van Pul, “Non-ohmic behavior of carbon black-loaded rubbers,” *Carbon N. Y.*, vol. 2, no. 2, pp. 121–126, Oct. 1964, doi: 10.1016/0008-6223(64)90051-X.

[44] T. Tamai, “Electrical Properties of Conductive Elastomer as Electrical Contact Material,” *IEEE Trans. Components, Hybrids, Manuf. Technol.*, vol. 5, no. 1, pp. 56–61, 1982, doi: 10.1109/TCHMT.1982.1135954.

[45] W. Bauhofer and J. Z. Kovacs, “A review and analysis of electrical percolation in carbon nanotube polymer composites,” *Compos. Sci. Technol.*, vol. 69, no. 10, pp. 1486–1498, 2009, doi: 10.1016/j.compscitech.2008.06.018.

[46] D. S. McLachlan *et al.*, “AC and DC percolative conductivity of single wall carbon nanotube polymer composites,” *J. Polym. Sci. Part B Polym. Phys.*, vol. 43, no. 22, pp. 3273–3287, 2005, doi: 10.1002/polb.20597.

[47] M. F. Yu, O. Lourie, M. J. Dyer, K. Moloni, T. F. Kelly, and R. S. Ruoff, “Strength and breaking mechanism of multiwalled carbon nanotubes under tensile load,” *Science (80-.).*, vol. 287, no. 5453, pp. 637–640, 2000, doi: 10.1126/science.287.5453.637.

[48] A. Nilchian and C. Z. Li, “Mechanical and electrochemical characterization of CNT/PDMS composited soft and stretchable electrodes fabricated by an efficient solution-based fabrication method,” *J. Electroanal. Chem.*, vol. 781, pp. 166–173, 2016, doi: 10.1016/j.jelechem.2016.08.013.

[49] S. Xie, W. Li, Z. Pan, B. Chang, and S. Lianfeng, “Mechanical and physical properties on carbon nanotube,” *J. Phys. Chem. Solids*, vol. 61, no. 7, pp. 1153–1158, 2000, doi: 10.1016/S0022-3697(99)00376-5.

[50] D. Ponnamma, K. K. Sadasivuni, Y. Grohens, Q. Guo, and S. Thomas, “Carbon nanotube based elastomer composites-an approach towards multifunctional materials,” *J. Mater. Chem. C*, vol. 2, no. 40, pp. 8446–8485, 2014, doi: 10.1039/c4tc01037j.

[51] Y. Y. Huang and E. M. Terentjev, “Tailoring the electrical properties of carbon nanotube-polymer composites,” *Adv. Funct. Mater.*, vol. 20, no. 23, pp. 4062–4068, 2010, doi: 10.1002/adfm.201000861.

[52] A. V Eletskii, A. A. Knizhnik, B. V Potapkin, and J. M. Kenny, “Electrical characteristics of carbon nanotube-doped composites,” *Physics-Uspekhi*, vol. 58, no. 3, pp. 209–251, 2015, doi: 10.3367/ufne.0185.201503a.0225.

[53] R. Andrews, D. Jacques, M. Minot, and T. Rantell, “Fabrication of carbon multiwall nanotube/polymer composites by shear mixing,” *Macromol. Mater. Eng.*, vol. 287, no. 6, pp. 395–403, 2002, doi: 10.1002/1439-2054(20020601)287:6<395::AID-MAME395>3.0.CO;2-S.

[54] Z. Q. Meng, R. T. Liu, Y. J. Xiong, F. A. Zhao, and X. Bin Li, “Effect of ball milling on morphology and structure of multi-walled carbon nanotubes,” *Zhongguo Youse Jinshu Xuebao/Chinese J. Nonferrous Met.*, vol. 22, no. 12, pp. 3421–3426, 2012.

[55] M. Inkyo, T. Tahara, T. Iwaki, F. Iskandar, C. J. Hogan, and K. Okuyama, “Experimental investigation of nanoparticle dispersion by beads milling with centrifugal bead separation,” *J. Colloid Interface Sci.*, vol. 304, no. 2, pp. 535–540, 2006, doi: 10.1016/j.jcis.2006.09.021.

[56] F. N. A. M. Sabri, M. R. Zakaria, and H. M. Akil, “Dispersion and stability of multiwalled carbon nanotubes (MWCNTs) in different solvents,” *AIP Conf. Proc.*, vol. 2267, no. September 2020, 2020, doi: 10.1063/5.0024711.

[57] A. Diekmann, M. C. V. Omelan, and U. Giese, “Influence of carbon nanotube-pretreatment on the properties of polydimethylsiloxane/carbon nanotube-nanocomposites,” *Polymers (Basel).*, vol. 13, no. 9, 2021, doi: 10.3390/polym13091355.

[58] R. Ramalingame, D. Rajendran, A. Lakshmanan, and O. Kanoun, “Effect of organic solvent on MWCNT-PDMS nanocomposite based capacitive pressure sensors,” *2018 15th Int. Multi-Conference Syst. Signals Devices, SSD 2018*, pp. 1208–1211, 2018, doi: 10.1109/SSD.2018.8570607.

[59] A. Nag, N. Afsarimanesh, S. Nuthalapati, and M. E. Altinsoy, “Novel Surfactant-Induced

MWCNTs/PDMS-Based Nanocomposites for Tactile Sensing Applications," *Materials (Basel).*, vol. 15, no. 13, 2022, doi: 10.3390/ma15134504.

[60] S. Xu, Z. Fan, C. Li, P. Wang, K. A. Sammed, and L. Pan, "Investigation of strain sensing mechanisms on the ultra-thin carbon nanotube networks with different densities," *Carbon N. Y.*, vol. 155, pp. 421–431, 2019, doi: 10.1016/j.carbon.2019.09.004.

[61] K. Chu and S. H. Park, "Electrical heating behavior of flexible carbon nanotube composites with different aspect ratios," *J. Ind. Eng. Chem.*, vol. 35, pp. 195–198, 2016, doi: 10.1016/j.jiec.2015.12.033.

[62] D. Zhu, S. Handschuh-Wang, and X. Zhou, "Recent progress in fabrication and application of polydimethylsiloxane sponges," *J. Mater. Chem. A*, vol. 5, no. 32, pp. 16467–16497, 2017, doi: 10.1039/c7ta04577h.

[63] S. C. B. Mannsfeld *et al.*, "Highly sensitive flexible pressure sensors with microstructured rubber dielectric layers," *Nat. Mater.*, vol. 9, no. 10, pp. 859–864, 2010, doi: 10.1038/nmat2834.

[64] S. R. A. Ruth and Z. Bao, "Designing Tunable Capacitive Pressure Sensors Based on Material Properties and Microstructure Geometry," *ACS Appl. Mater. Interfaces*, vol. 12, no. 52, pp. 58301–58316, 2020, doi: 10.1021/acsami.0c19196.

[65] S. R. A. Ruth, L. Beker, H. Tran, V. R. Feig, N. Matsuhisa, and Z. Bao, "Rational Design of Capacitive Pressure Sensors Based on Pyramidal Microstructures for Specialized Monitoring of Biosignals," *Adv. Funct. Mater.*, vol. 30, no. 29, pp. 1–12, 2020, doi: 10.1002/adfm.201903100.

[66] S. R. A. Ruth, V. R. Feig, H. Tran, and Z. Bao, "Microengineering Pressure Sensor Active Layers for Improved Performance," *Adv. Funct. Mater.*, vol. 30, no. 39, pp. 1–31, 2020, doi: 10.1002/adfm.202003491.

[67] J. O. Kim *et al.*, "Highly Ordered 3D Microstructure-Based Electronic Skin Capable of Differentiating Pressure, Temperature, and Proximity," *ACS Appl. Mater. Interfaces*, vol. 11, no. 1, pp. 1503–1511, 2019, doi: 10.1021/acsami.8b19214.

[68] F. Cote, R. Biagi, H. Bart-Smith, and V. S. Deshpande, "Structural response of pyramidal core sandwich columns," *Int. J. Solids Struct.*, vol. 44, no. 10, pp. 3533–3556, 2007, doi: 10.1016/j.ijsolstr.2006.10.004.

[69] J. M. Martínez, C. Delso, D. Aguilar, G. Cebrián, I. Álvarez, and J. Raso, "Factors influencing autolysis of Saccharomyces cerevisiae cells induced by pulsed electric fields," *Food Microbiol.*, vol. 73, pp. 67–72, 2018, doi: 10.1016/j.fm.2017.12.008.

[70] Formlabs, "Intro to Stereolithography 3D Printing," 2019. https://formlabs.com/uk/blog/ultimate-guide-to-stereolithography-sla-3d-printing/.

[71] P. S. Vernon and A. H. Rose, "Adsorption of silicon antifoam by Saccharomyces Cerevisiae," *J. Inst. Brew.*, vol. 82, no. 6, pp. 336–340, Nov. 1976, doi: 10.1002/j.2050-0416.1975.tb06958.x.

[72] C. Parameswaran and D. Gupta, "Low cost sponge based piezocapacitive sensors using a single step leavening agent mediated autolysis process," *J. Mater. Chem. C*, vol. 6, no. 20, pp. 5473–5481, 2018, doi: 10.1039/c8tc00972d.

[73] C. Parameswaran, R. P. Chaudhary, S. Hosangadi Prutvi, and D. Gupta, "Rapid One Step Fabrication of Hydrophilic Hierarchical Porous PDMS with Negative

Piezopermittivity for Sensing and Energy Storage Applications," *ACS Appl. Polym. Mater.*, vol. 4, no. 3, pp. 2047–2056, 2022, doi: 10.1021/acsapm.1c00593.

[74] J. K. W. Sandler, J. E. Kirk, I. A. Kinloch, M. S. P. Shaffer, and A. H. Windle, "Ultra-low electrical percolation threshold in carbon-nanotube-epoxy composites," *Polymer (Guildf).*, vol. 44, no. 19, pp. 5893–5899, 2003, doi: 10.1016/S0032-3861(03)00539-1.

[75] J. M. Watson and M. G. Baron, "The behaviour of water in poly (dimethylsiloxane)," vol. 110, pp. 47–57, 1996.

[76] S. Vudayagiri, M. D. Junker, and A. L. Skov, "Factors affecting the surface and release properties of thin polydimethylsiloxane films," *Polym. J.*, no. November 2012, pp. 871–878, 2013, doi: 10.1038/pj.2012.227.